Chapter 14
Adaptive Specular Reflection Detection in Cervigrams (ASRDC) Technique: A Computer-Aided Tool for Early Screening of Cervical Cancer

Brijesh Iyer and Pratik Oak

14.1 Introduction

Cervical cancer (CC) is the fourth most recurrent women's cancer worldwide. In line with the WHO health report, every fifth woman in the world will be impacted by it in 2050 [1]. Nearly 90% of the 270,000 deaths from CC in 2015 took place in low- and middle-income countries. Noteworthy progress in disease screening and treatment supports prevention, and prompt diagnosis may drastically reduce the CC mortality rate [1].

CC begins with abnormal modifications in the cervical tissue. The risk of having these unusual changes is concomitant with infection by the human papillomavirus (HPV). Moreover, early sexual interaction, manifold sexual partners, usage of oral contraceptives (birth control pills), unhygienic lifestyle, and misinformation are the critical factors for spreading this disease. If spotted early, CC can be cured reasonably. The most prevalent CC detection method is the Pap smear.

Nonetheless, it has inherent limitations such as sample quality, slide quality, and effectiveness of screeners. The CAD systems can help to treat this disease by analyzing an input image and, with the assistance of various image-processing algorithms, predict or detect abnormalities. The earliest and challenging step in medical image exploration is to pre-process the input image for the uncovering and removal of noise. Specular reflection (SR) is a variety of prominent noise that appears in photography and medical imaging. Once a ray of light strikes the surface, a portion of the ray is straightaway reflected from the interface amid the surface and the air, thanks to their different refractive indices. This reflected light is called SR [2]. The humidity on the cervix surface engenders the SR, which hampers early CC

B. Iyer (✉) · P. Oak
Department of E&TC Engineering, Dr. Babasaheb Ambedkar Technological University, Lonere, India
e-mail: brijeshiyer@dbatu.ac.in

A. Khelassi, V. V. Estrela (eds.), *Advances in Multidisciplinary Medical Technologies ─ Engineering, Modeling and Findings*,
https://doi.org/10.1007/978-3-030-57552-6_14

Fig. 14.1 Example of an SR affected cervix image with cropped SR region

detection by computational systems [3]. Figure 14.1 illustrates the initial cervix image with the SR region (black box in the middle) and cropped SR region near it so that these regions undergo automatic detection, correction, and deletion according to the specialist's needs.

The rest of the manuscript goes as follows: Sect. 14.2 talks over the state-of-the-art methods for SR detection and its removal. Section 14.3 describes the components of the ASRDC scheme. The experimental outcomes appear in Sect. 14.4. Section 14.5 closes this work with remarks on the ASRDC methodology and its future.

14.2 State-of-the-Art Technology

Automatic recognition and removal of SR experimented a few contributions lately. The correlated literature generally embraces four categories as (i) the dichromatic reflection model (DRM) usage, (ii) kernel filtering, (iii) SR cast as classification, and (iv) thresholding procedures.

The DRM principle states that a reflection combines specularity and diffusion linearly. Yoon et al. appraised the value of the specularity-invariant pixels as well as their ratio to set apart diffuse components. Still, this maneuver suits textured imageries, and approximation in the normalization procedure bounds the accuracy of SR detection [4]. Tao et al. introduced a new metric termed line consistency for depth estimation of specular regions. They had estimated colors from multiple light sources. However, this strategy failed to distinguish saturated specularity [5]. J Suo et al. applied the DRM rationale perceiving the problem as a signal separation for SR detection and removal.

In contrast, the procedure overlooked smooth color alterations, and it failed to discern the pixels with identical hue and different saturation [6–8]. Das et al. advised kernel-based filters for SR detection and exclusion, e.g., filling, dilation, multiscale morphology, and IS-histogram [3]. Kudva et al. utilized morphological kernels as filters to acquire features from color images [9]. Xue et al. predefined the structuring element (SE) as a kernel. The top-hat transform treated the intensity image I (whose entries hold brightness values within some range) of input cervigrams [10]. Yet, all these schemes rest on the size and shape of the kernel applied to the database. Gao et al. proposed SR detection as a classification problem using SVM classifiers. This method's caveat is the requirement of training every time for SR detection [11].

Zimmerman et al. suggested multiplying S and I by an arbitrary constant where S is the saturation component, which shows how much the white color taints a given color. The S component belongs to the range [0, 1] within the HSI plane. The gradient image outputs on these multiplied regions are SR pixels [12]. Akbar et al. computed the SR pixel via a chaotic clonal selection procedure [13]. The image specular degree can function as a thresholding parameter to separate diffused images and for SR detection [2, 14]. The choice of arbitrary constants throughout automatic detection of SR pixels may be contingent on the database under experimentation. However, the detection system must be entirely automated and independent of the database. Therefore, any imaging modality calls for automatic threshold selection. Table 14.1 relates the state-of-the-art SR discovery approaches and the ASRDC concept. Automatic thresholding fits in fivefold groups according to the information content they rely upon, viz.:

(i) Histogram-based schemes analyze the primary intensity, decimation in intensity range, and nonlinear nature of the smoothed histogram.
(ii) Clustering-related strategies split the gray levels from the input image into the background and foreground pixels.
(iii) Entropy-based methods employ local entropy, cross-entropy of the foreground and background regions, original and binary images, etc.

Table 14.1 State-of-the-art SR detection categories

Sr. No.	Category	Working principle	Remarks
1.	Dichromatic reflection model [4–7]	Reflection is a linear combination of specular and diffuse components	Limits the identification of saturated specularity
2.	Use of kernel as a filter [3, 9, 10]	Applying a specific mask on an input image as a filtering operator	The inappropriate selection of size and shape of the kernel affects the accuracy
3.	SR as a classification problem [11]	Feature extraction and training a system with predefined labels as SR pixels	Requires a training system every time for SR detection
4.	Thresholding [2, 3, 12, 13]	Collection of pixels falling below the predefined threshold value, as SR pixels	Arbitrary selection of constant makes the system database dependent
5.	ASRDC method	SR detection using automatic thresholding and quality enhancement of low-resolution images	Fully automatic system, which is independent of size and shape of kernel and selection of arbitrary constant, no need for separate training

(iv) Object attribute-based methods focus on the similarity between the gray level and its black and white versions.
(v) Statistical relation-founded schemes rely on higher-order moments and/or the correlation among pixels for threshold selection [15].

These threshold-picking strategies can be either bi-modal or multi-modal. Nonetheless, the application demands to get SR pixels, which are always bright. Hence, bi-modal distribution is the best choice, along with a histogram-based approach. Table 14.2 abridges a review of automatic threshold determination practices built on histograms.

In 2004, Sezgin and Sankur reviewed the performance of thresholding techniques using five quality measures, viz., misclassification error (ME), edge mismatch (EMM), relative foreground area error (RAE), modified Hausdorff distance (MHD), and region nonuniformity (NU). They calculated the average score of each scheme, ranked individual quality measures, and, finally, concluded that Kittler and Kapura were the superlative adaptive thresholding procedures [15]. Donald Bailey also investigated adaptive thresholding techniques for performance analysis and

Table 14.2 State-of-the-art SR detection categories

Author	Criteria function	Significance	Remarks
Calvard and Riddler [16]	Starts with the histogram mean Updates the threshold with the average of the lower and upper means of the histogram. Stops if the lower and upper threshold difference is zero	Simple and speedy Detected threshold is useful for foreground separation	SR intensities are always brighter Not suitable for SR detection
Otsu [17]	Use of kernel [3, 9, 10], minimizing intra-class variance between the left and right regions of the histogram	Best suitable for histograms with a clear valley between the modes	Not suitable for histograms where objects and b/g are not well separated
Kapura [18]	Maximization of entropy between two regions	Works on actual information extraction of two modes	SR detection does not require to know average information of lower-intensity pixel region
Kittler [19]	Minimum error thresholding for the standard deviation of both sub-histograms	Moderate threshold selection. Suitable for proper foreground detection	Some changes in partitioning required for high-intensity threshold selection
Carlotto [20]	Histogram represented as the combination of Gaussian mixtures of different modes	Approximation of histogram is dependent for the selection of the number of modes	Computationally complex
Patra [21]	Calculated energy of pixel over a 3×3 neighborhood	Proposed energy curve behaving similar to a histogram with valleys and peaks	Applicable for spatial contextual information inappropriate for multilevel histogram

found that Kittler's minimum error is the best [20]. The ASRDC methodology overcomes the limitations above due to:

(a) Its complete independence on size and shape of the kernel
(b) No requirement for the training process
(c) Fully automatic threshold calculations

The catchline features of the ASRDC methodology are:

1. Use of the lightness as a no-reference quality measure for selection of appropriate algorithm
2. Automatic selection of threshold by a modified Kittler's method
3. Automatic enhancement of low-quality images before the SR treatment

14.3 The ASRDC Methodology

The ASRDC block diagram appears in Fig. 14.2. The section further describes the threefold contribution of the chapter.

14.3.1 Selection of Optimum Threshold Detection Technique

The authors picked the Kittler minimum error thresholding scheme for automatic SR detection [19] from the approaches talked over in Sect. 14.1.

14.3.2 Automatic SR Detection

A histogram exemplifies the distribution of the pixel intensities, where an SR is a bright spot on an image, which agrees with the maximum part of the intensity range (close to white). Nevertheless, few non-SR pixels may also possess high brightness. SR pixels occur at the dark side of the ***S*** in addition to the bright side of the ***I*** images

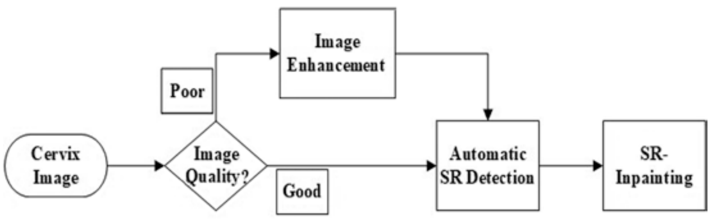

Fig. 14.2 Block diagram of the ASRDC system

[14]. As a consequence, the SR occurrence in the intensity saturation (IS) histogram is a foremost ASRDC concern. The automatic SR recognition is carried out by a simple variant of the Kittler method to attain the optimum threshold on the ***S*** and ***I*** images. The modified Kittler method (MKM) understands the threshold (*T*) differently from the original tactic. This work considers the span going from minimum to maximum intensity (i.e., over complete dynamic range) as opposed to starting with a random *T*. An optimum threshold matches the minimum Jaccard Index (JI) value (aka criteria function) of the MKM.

The Jaccard Index *J* is a statistic that explains the similarities between finite sample sets. *J* is defined properly as

$$J = \frac{|A \cap B|}{|A \cup B|} = \frac{|A \cap B|}{|A| + |B| - |A \cap B|}, \tag{14.1}$$

i.e., the size of the intersection $|A \cap B|$ divided by the size of the union $|A \cap B|$ of the sample sets *A* and *B*.

The ASRDC methodology employs half of the intensities for two different inputs. The thresholds, starting from 1 to 128, assist in calculating the minimum error with the MKM criterion function and are known as the left-side threshold (*TL*). Similarly, the right-side threshold (*TR*) results from all combinations of pixels from 128 to 256. The modified algorithm is given below.

The MKM Algorithm

1. Go through every possible threshold (T), i.e., grey level from 1 to 128 or from 128 to 256.
2. Consider the groups (i) 1 or T, and (ii) 2 or (T+1), i.e., highest intensity.
3. Compute the histograms of these groups and mark their sums as P1 and P2.
4. Determine the mean and standard deviation for the histograms.
5. Compute the Jaccard Index (J) criterion function for all possible T.
6. The finishing threshold is the position with minimum J.

Thresholds generated from step 6 (*TL* and *TR*) work on saturation (***S***) and intensity (***I***) images, respectively. The SR pixels as given below.

$$SR = \left(S(i,j) < TL\right) \&\& \left(I(i,j) > TR\right) \tag{14.2}$$

where (*i*, *j*) symbolizes the pixel location (for row *i* and column *j*) in an picture and “&&” is the logical AND.

14.3.3 Image Quality Assessment (QA)

The overall input image condition dramatically impacts any algorithm performance. Therefore, the input image quality assessment (QA) is vital to the deployment of an adaptive system. The objective QA of the examined picture consists of the computation of the threefold quality metric categories, viz., full reference (FR), reduced reference (RR), and no reference (NR). As ground reality images are not available when it comes to cervigrams, the NR metric is preferred in input quality testing. Several investigators commended many color quality parameters or attributes for NR-based QA like brightness, colorfulness, sharpness, contrast, and entropy. The colorfulness illustrates the color information perceived by the human eye. The sharpness gives the amount of preservation of edges. The contrast addresses the emphasis on the foreground and background association. The average image information corresponds to the brightness measures, whereas the lightness promotes the distortion in intensities of pixels [22].

It is essential to use quality measures related to distortion for SR detection. Hence, the ASRDC scheme takes account of the lightness parameter together with colorfulness (C1), contrast (C2), and sharpness (C3). Their grouping forms a quality measure if and only if they are correlated, which, consequently, leads to the calculation of the correlation between the lightness and the three attributes. The validation of the null hypothesis can confirm the possibility of this combination, i.e., the lightness is uncorrelated with all three attributes. The Pearson correlation coefficient (p-value) gives the acceptance probability of the null hypothesis. In general, the significance level of the p-value is 0.05, namely, if the p-value is less than 0.05, attributes are correlated with the refutation of the null hypothesis [23]. The tryouts from Sect. 14.4 (B) substantiate the dominance of lightness features among the color attributes to deal with an eventual image enhancement. The experimental investigation of the ASRDC method indicates that if the lightness is greater than 1, then image quality amelioration is required.

The low-quality images must be enhanced before applying the ASRDC methodology. This scheme has a histogram-based automatic threshold selection (Sect. 14.3 (B)) that also enhances pictures by altering the histogram shape.

Most prevalent histogram-centered measures to enhance pictures are histogram equalization (HE) [17], bi-HE (BHE) [24], adaptive HE (AHE) [32], contrast-limited AHE (CLAHE) [33], and brightness preserving BHE (BBHE) [24]. Among these approaches, the BBHE scheme preserves the image characteristics after preprocessing. Hence, this work treated low-quality images with BBHE before employing the ASRDC method to manage SR in an input image adaptively as:

(a) Initial quality check of the input picture utilizing the lightness parameter
(b) Low-quality image enhancement through BBHE
(c) Application of the ASRDC technique to the input image

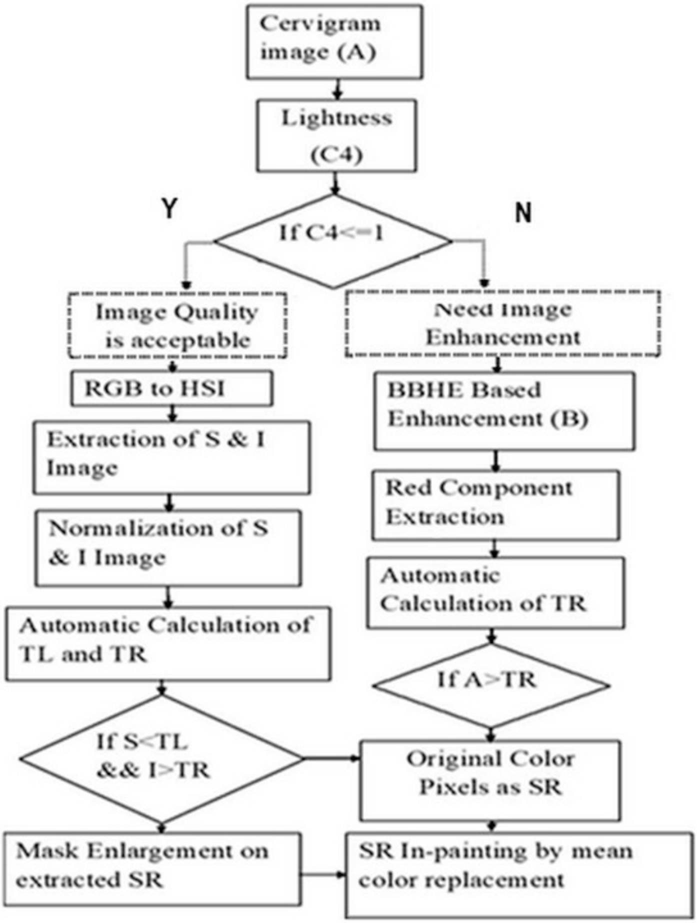

Fig. 14.3 ASRDC workflow

14.3.4 SR Inpainting

Further SR inpainting is carried out to generate the SR free image. An iterative non-zero averaging filter creates an SR free image [10]. The complete flow of the ASRDC method arises in Fig. 14.3 with its algorithm.

ASRDC Algorithm

1. Take the input cervix image and calculate the lightness.
2. If lightness < 1,
   - (i) RGB to HSI conversion to separate saturation (***S***) and intensity (***I***) images
   - (ii) Compute left (TL) and right threshold (TR) using the ASRDC method
   - (iii) Collect pixels lying between intensities of ***S*** less than TL and intensities of ***I*** greater than TR, as SR pixels
   - (iv) Perform mask enlargement on the output of step 2 (iii)
3. If lightness > 1, Apply BBHE on the input image and extract red component
   - (i) Calculate TR from BBHE image
   - (ii) Collect pixels of the input image which are greater than TR, as SR pixels
4. Inpaint detected SR pixels by mean color replacement.

14.4 Results and Discussions

14.4.1 The Dataset

The present exploration involves digitized uterine cervix pictures collected by the National Cancer Institute (NCI) from four epidemiological studies made in the USA, e.g., "Costa Rican Natural History Study of HPV and Cervical Neoplasia (NHS)," "ASCUS LSIL Triage Study (ALTS)," "Biopsy Study," and "Costa Rica Vaccine Trial (CVT)" on HPV and CC screening [25]. The trials comprise a total of 612 images from all 4 datasets distributed as NHS (200), ALTS (200), Biopsy (50), and CVT (162). This research work selects images randomly from the available databases with resolutions for pictures in the ALTS and NHS equal to 2891 × 1973 and for the Biopsy and CVT, 4256 × 2832.

The acceptance of the image enhancement output entails the evaluation of the quality of the input image. As talked over in Sect. 14.3.3, the *p*-value is calculated to obtain the correlation between image attributes. Table 14.3 displays the p-values for various arrangements of images from the datasets.

Table 14.3 *p*-values between C4 and C1, C2, and C3

	p-value		
Dataset	C4-C1	C4-C2	C4-C3
ALTS + Biopsy (21 images)	0.1577	0.0487	$\mathbf{1.29 \times 10^{-6}}$
ALTS + Biopsy + CVT (61 images)	0.1195	0.1401	$\mathbf{7.73 \times 10^{-9}}$
All 4 datasets (113 images)	0.006	0.309	$\mathbf{1.64 \times 10^{-11}}$

C1, C2, C3, and C4 represent the colorfulness, sharpness, contrast, and lightness attributes, respectively. The p-values of C3 are very low (i.e., <0.05 for all combinations of the dataset). However, C1 and C2 show significant p-values concerning the significance level. This implies a correlation between lightness and contrast. Thus, the lightness can be combined with contrast to test the image quality. The present analysis selected 80 images (20 from each dataset) to determine the dominant feature between lightness and contrast. This experiment aims to confirm the necessity of image enhancement through no-reference image attribute. The contrast of all 80 images ranges between 0.45 and 0.5, which did not give a noteworthy threshold as a decision parameter. However, a significant change in the value of lightness is observed for all 80 images, as below and above value 1. Thus, lightness is chosen as a dominant feature of the cervix color image to decide the input quality. Experimentation concluded the adaptability condition as if the lightness is less than 1, input image quality is satisfactory, and the ASRDC algorithm should get applied without image enhancement. For an image with lightness greater than 1, it should be enhanced before applying the ASRDC algorithm.

14.4.2 Experiments

The ***S*** and ***I*** images are normalized to the original grayscale range of 0 to 255. *TL* is calculated for the ***S*** image, and *TR* is calculated for ***I*** the image, as explained in Sect. 14.3.2. The original Kittler method and the MKM are applied to normalized ***S*** and ***I*** images. The final SR pixels are detected using Eq. 14.2. Table 14.4 compares the average threshold for ***S*** and ***I*** images using both methods. The thresholds given by the original Kittler method show nonuniformity over different sets of cervix images and detect a very less number of SR pixels. This affects the accuracy of SR pixel detection. However, the approximate range of difference between *TL* and *TR* by the suggested modification (*TR-TL* = dynamic range of intensities of non-SR pixels) is constant for all four datasets under experimentation. This, in turn, increases the accuracy of SR as well as non-SR pixel detection.

The SR is detected using the recommended modification explained in Sect. 14.3.2 (Fig. 14.4) that contemplates the fact that the SR pixels are heterogeneous regarding other image pixels and that they can be easily observed by the human eye. The performance of enhancement relying on SR detection for low-quality images

Table 14.4 Average left-side and right-side threshold

	Threshold for ***S*** image (***TL***)		Threshold for ***I*** image (***TR***)	
Database	Original image	Proposed method	Original image	Proposed method
ALTS	16.4	63.38	253	165.4
Biopsy	68	69.78	88.85	157.7
CVT	73.05	45.11	107.8	163
NHS	24.4	28.5	227.9	179.1

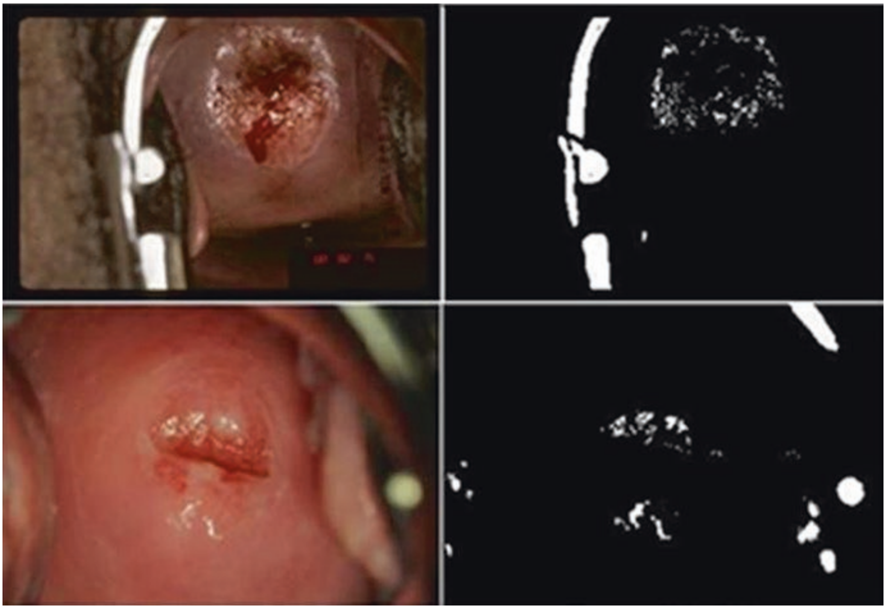

Fig. 14.4 SR pixel detection

Fig. 14.5 Performance of enhancement-based SR detection for low-quality image

corroborates the prerequisite of adaptability from Sect. 14.3.4. Figure 14.5b shows the detected SR pixels from the original low-quality image, whereas accurate SR detection from the enhanced high-quality image after the ASRDC application appears in Fig. 14.5c showing that the SR detection is effective to the adaptive enhancement of the low-quality image.

14.4.3 SR Inpainting

The iterative mean color replacement from Sect. 14.3.2 takes away the detected SR pixels (refer to Fig. 14.6). The ASRDC method adaptively selects the SR detection tactic to be applied with or without input image enhancement based on the lightness

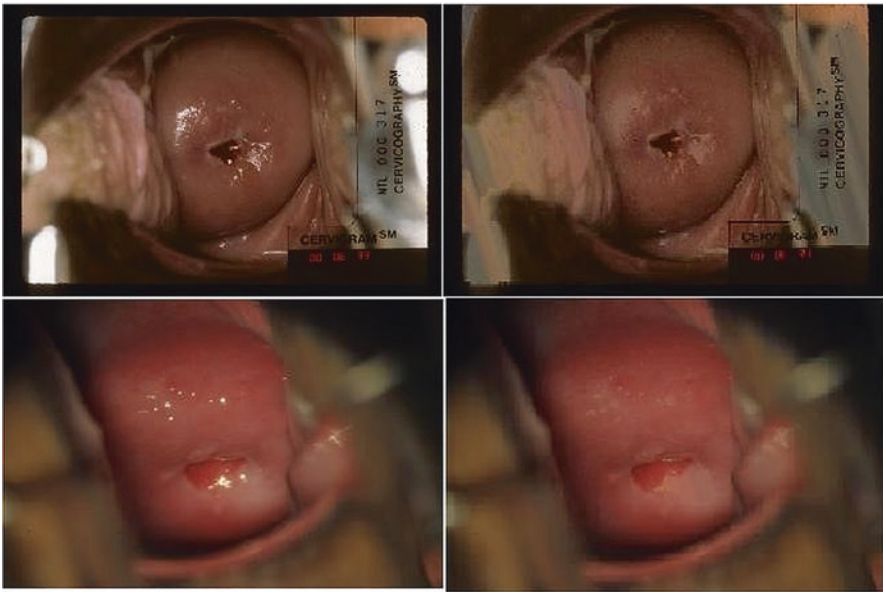

Fig. 14.6 SR Inpainting using mean color replacement

measure of an image. The enhancement initiates automatically for low-quality images before applying the ASRDC technique.

14.4.4 Quantitative Evaluation of Proposed Method

Most of the reported literature spoke about visual comparisons of various SR detection and removal methods [3–5, 13, 14, 17]. Due to the unavailability of ground reality images captured with proper illumination, the quantitative evaluation is complicated.

However, the ASRDC system compares results utilizing NR image quality attributes of the original and inpainted image on the dataset under experimentation. Table 14.5 provides the average calculations of mean and standard deviation, respectively. It proves that an inpainted image has a low mean as compared to the original image that is to say SR (bright intensity pixels) are removed. The SR free image is homogeneous due to uniformity in image intensities and has less deviation from the mean, i.e., a decrease in the standard deviation. Table 14.6 illustrates the attributes of color image, viz., colorfulness, sharpness, and standard deviation. The SR removal decreases the colorfulness due to mean color replacement, makes the input image sharper, and decreases the proportion of distortion present in the input image, i.e., decrease in lightness. These observations depict a close agreement with the theoretical concepts of NR color image quality metrics.

Table 14.5 Comparison of statistical characteristics of original and inpainted image

		Mean	Standard deviation	
Database	Original image	Inpainted image	Original image	Inpainted image
ALTS	66.7	55.31	57.49	39.99
Biopsy	73.52	72.56	42.06	40.58
CVT	81.82	71.35	42.59	40.58
NHS	75.38	64.13	60.8	48.8

Table 14.6 Comparison of color image attributes of original and inpainted image

Quality measure/ database	Colorfulness		Sharpness		Lightness	
	Original image	Inpainted image	Original image	Inpainted image	Original image	Inpainted image
ALTS	1.378	1.276	0.415	0.662	1.28	1.08
Biopsy	1.564	1.512	0.475	0.748	1.002	0.97
CVT	1.373	1.272	0.392	0.689	1.002	0.94
NHS	1.588	1.496	0.489	0.619	1.22	1.09

14.4.5 Qualitative Analysis for State-of-the-Art Methods

Figure 14.7 illustrates the comparative visual difference between the ASRDC method and other state-of-the-art implementations aiming at SR detection and mitigation suggested in [9, 12, 14]. It follows that the novel ASRDC technique outsmarts the reported practices in terms of SR detection for images collected from different databases. Kudva et al. suggested the use of the Jaccard Index (JI) to measure the quantitative performance of SR detection techniques with manually marked SR pixels for images having practically visible SR pixels [9]. The JI value must be higher for the selected image to have accurate detection.

Table 14.7 parallels outcomes for the maximum JC for the ASRDC scheme and other state-of-the-art techniques to validate the new approach. The present analysis considered only four images for the JC evaluation. However, the method can be extended for the entire database assessment. Recently, efforts relying on artificial intelligence (AI), data mining, and fuzzy-based methodologies addressed the SR detection issue [26, 27]. Health 4.0 protocols have also provided new insights regarding the usage of medical resources to handle various medical emergencies [28–31]. These lines of attack may lead to a revolution in CC detection and treatment.

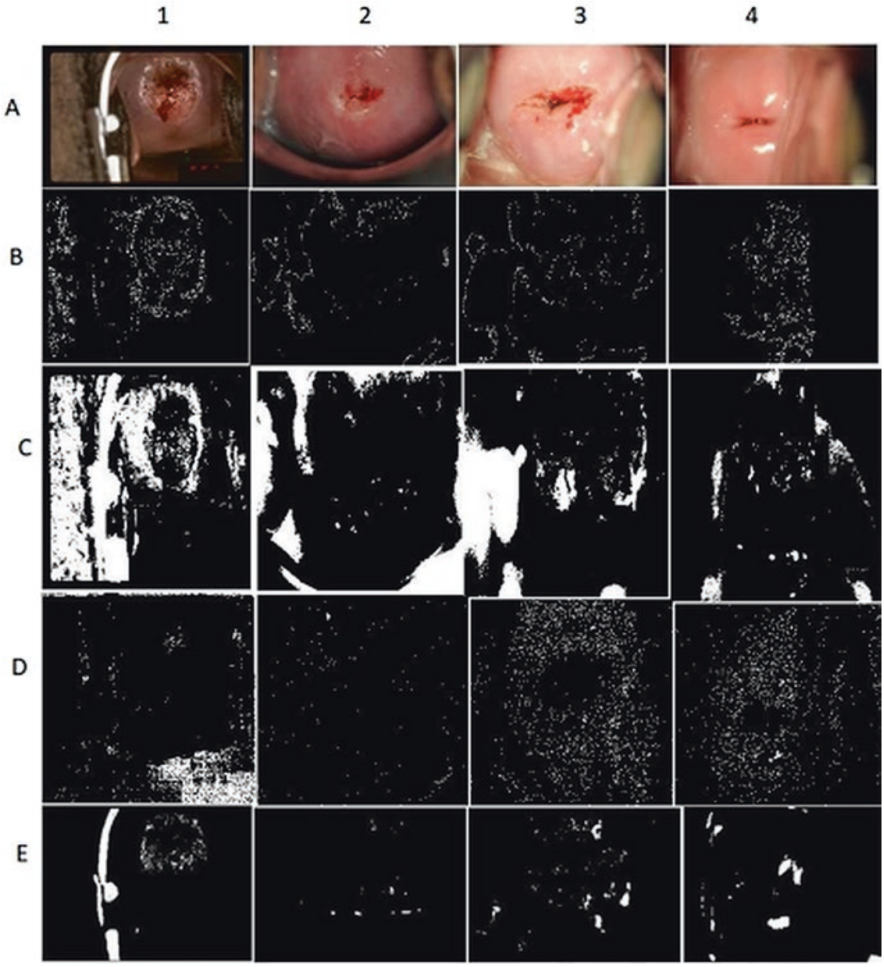

Fig. 14.7 Comparative analysis of state-of-the-art methods for SR detection. (**a**) Original image; (**b**) SR detection with [12]; (**c**) SR detection using [14]; (**d**) SR detection via [9]; (**e**) SR detection using the ASRDC method

Table 14.7 Qualitative analysis with state-of-the-art methods of SR detection

Image	JC using [12]	JC using [14]	JC using [9]	JC for the ASRDC method
1	0.0033	0.0413	0.0099	**0.1005**
2	0.0041	0,1737	0.0852	**0.4923**
3	0.0012	0.1334	0.0282	**0.3571**
4	0.0029	0.2208	0.0421	**0.4695**

14.5 Conclusions

This research puts forward the ASRDC as an adaptive method for detection and removal of SR from input cervix image, i.e., cervigrams. Experimentation was carried out on 612 images collected from NCI. The ASRDC method overcomes significant limitations of current SR detection techniques, i.e., dependency on shape and size of the kernel, selection of arbitrary constant, and every time training of the system. The ASRDC methodology uses the lightness as an NR quality measure to check the necessity of image enhancement, automatic enhancement of low-quality images before SR detection technique, and automatic selection of threshold by the MKM. Subjective and objective quality evaluation over different datasets highlights the ASRDC significance. Noise and resolution of the biomedical image largely depend on the quality of the equipment used for the capture and the skills of the expert (human intervention). In general, noise content and resolution of any biomedical images can be improved by using equipment that is more sophisticated. In addition to this, the ASRDC methodology will be an additional tool to enhance the grade of the biomedical images under study.

The inpainted images generated by the ASRDC adaptive system can be passed to further stages of early CC detection for additional feature extraction, segmentation, and classification techniques.

The authors are aware that when it comes to analyses of 3D images and 2D or 3D video, other shortcomings may affect SR detection as well as correction. For the cases when the dimensionality is high and several imaging modalities become necessary, soft computing strategies may lessen the processing time, help with more challenging settings, and work with other objective metrics [32–42]. It should be pointed out that SR detection and removal can benefit from the knowledge obtained in other similar image-processing tasks that share some characteristics and caveats with this problem.

Acknowledgments The authors gratefully acknowledge support from Dr. M. Schiffman and the team of the National Cancer Institute for providing the data from NCI Guanacaste and ALTS projects.

Ethical Approval This article does not contain any studies with human participants or animals, performed by any of the authors.

Funding The work reported in this manuscript does not receive any funding from any source/agency.

References

1. WHO cervix cancer report. Available at: http://www.who.int/cancer/prevention/diagnosis-screening/cervical-cancer/en
2. H. Shen et al., Simple and efficient method for specularity removal in an image. Appl. Opt. **48**(14), 2711–2719 (2009)

3. A. Das et al., Elimination of specular reflection and identification of ROI: The first step in automated detection of cervical cancer using digital colposcopy. In: IEEE International Conference on Imaging Systems and Techniques, 237–241 (2011)
4. K. Yoon et al., Fast separation of reflection components using a specularity invariant image representation. In: Proceedings of IEEE International Conference on Image Processing, 973–976 (2006)
5. M. Tao et al., Depth estimation and specular removal for glossy surfaces using point and line consistency with light-field cameras. IEEE Trans. Pattern Anal. Mach. Intell. **38**(6), 1155–1169 (2016)
6. J. Suo, D. An, X. Ji, H. Wang, Q. Dai, Fast and High Quality Highlight Removal from a Single Image. IEEE Trans. Image Process. **25**(11), 54415454 (2016)
7. N. Lamprinou et al., Fast detection and removal of glare in gray scale laparoscopic images. In: Proceedings of the 13th international joint conference on computer vision, imaging and computer graphics theory and applications 4, 206–212 (2018)
8. K. Panetta, G. Chen, A. Sos, No reference color image contrast and quality measures. IEEE Trans. Consum. Electron. **59**(3), 643–651 (2017)
9. V. Kudva, K. Prasad, S. Guruvare, Detection of specular reflection and segmentation of cervix region in uterine cervix images for cervical cancer screening. IRBM **38**(5), 281–291 (2017)
10. X. Zhiyun et al., Comparative performance analysis of cervix ROI extraction and specular reflection removal algorithms for uterine cervix image analysis. In: Proceedings of SPIE Medical Imaging, 6512 (2007)
11. G. Yefei et al., Dynamic searching and classification for highlight removal on endoscopic image. In: International Congress of Information and Communication Technology, 762–776 (2017)
12. Z. Gali, G. Hayit, Automatic Detection of Specular Reflections in Uterine Cervix Images. In: Proceedings of SPIE Medical Imaging, 6144, 2037–2045 (2006)
13. H. Akbar, N. Herman, Removal of highlights in dichromatic reflection objects using segmentation and inpainting. In: International Conference on Robotics, Automation and Sciences (ICORAS), 1–4 (2016)
14. S. Alsaleh et al., Automatic and robust single-camera specular highlight removal in cardiac images: 37th Annual International Conference of the IEEE Engineering in Medicine and Biology Society (EMBC), 675–678 (2015)
15. S. Mehmet, S. Bulent, Survey over image thresholding techniques and quantitative performance evaluation. J. Electron. Imag **13**(1), 146–165 (2004)
16. T. Ridler, S. Calvard, Picture thresholding using an iterative selection method. IEEE Trans. Syst. Man Cybern. **8**(8), 630–632 (1978)
17. R. Gonzales, C. Woods, Digital Image Processing. 2nd Edition Wesley, an imprint of Pearson Education, 598–608 (2000)
18. J. Kapur, P. Sahoo, A. Wong, A new method for grey level picture thresholding using entropy of the histogram. IEEE Trans Comp. Vis. Graph. & Image Process. **29**(3), 273–285 (1985)
19. J. Kittler, J. Illingworth, Minimum error thresholding. IEEE J Pattern Recog **19**(1), 41–47 (1986)
20. D. Bailey, *Histogram operations*, 1st edn. (John Wiley and Sons (Asia) Pte. Ltd., 2011)
21. S. Patra, R. Gautam, A. Singla, A novel context sensitive multilevel thresholding for image Segmentation. Appl. Soft Comput. **23**, 122–127 (2014)
22. M. Osadebey, M. Pedersen, D. Arnold, W. Katrina, No-reference quality measure in brain MRI images using binary operations, texture and set analysis. IET Image Process. **11**(9), 672–684 (2017)
23. D. Lee, Alternatives to p value: Confidence interval and effect size. Korean J. Anesthesiol. **69**(6), 555–562 (2017)
24. K. Yeong, Contrast enhancement using brightness preserving Bi histogram equalization. IEEE Trans Consum Electron **43**(1), 1–8 (1997)
25. R. Herrero, M. Schiffman, Design and methods of population based natural history study of cervical neoplasia in rural Costa Rica: The Guanacaste Project. Pan Am. J. Public Health **1**(5), 362–375 (1997)

26. P. Oak, B. Iyer, Specular reflection detection for early prediction of cervix cancer. Lecture Note. Electr. Eng. **569**, 683–691 (2020)
27. P. Oak, B. Iyer, Specular reflection detection and substitution: A key for accurate medical image analysis. Lecture Note. Electr. Eng. **570**, 223–241 (2020)
28. A. Khelassi, *Artificial reasoning systems: Theory and medical applications* (Lambert Academic Publishing (LAP), Saarbrücken, 2013)
29. A. Khelassi, RAMHeR: Reuse and mining Health 2.0 resources. Electron. Physician **7**(1), 969–970 (2015)
30. A. Khelassi, C. Amine, Cognitive amalgam with a distributed fuzzy case-based reasoning system for an accurate cardiac arrhythmias diagnosis. Int. J. Inf. Commun. Technol. **7**(4/5), 348–365 (2015)
31. V.V. Estrela, A.C.B. Monteiro, R.P. França, I. Yuzo, A. Khelassi, N. Razmjooy, Health 4.0: Applications, management, technologies and review. Med Technol J **2**(4), 262–276 (2019)
32. P. Musa, F.A. Rafi, M. Lamsani, A review: Contrast-Limited Adaptive Histogram Equalization (CLAHE) methods to help the application of face recognition. 2018 Third International Conference on Informatics and Computing (ICIC), 1–6 (2018)
33. S. Yelmanov, O. Hranovska, Y. Romanyshyn, A new approach to the implementation of histogram equalization in image processing. 2019 3rd International Conference on Advanced Information and Communications Technologies (AICT), 288–293 (2019)
34. A.C.B. Monteiro, R.P. Franca, V.V. Estrela, S.R. Fernandes, A. Khelassi, R.J. Aroma, K. Raimond, Y. Iano, A. Arshaghi, UAV-CPSs as a test bed for new technologies and a primer to Industry 5.0, in *Imaging and sensing for unmanned aircraft systems*, ed. by V. V. Estrela, J. Hemanth, O. Saotome, G. Nikolakopoulos, R. Sabatini, vol. 2, 1, (IET, London, 2020), pp. 1–22
35. A. Deshpande, P. Patavardhan, V.V. Estrela, N. Razmjooy, Deep learning as an alternative to super-resolution imaging in UAV systems, in *Imaging and sensing for unmanned aircraft systems*, ed. by V. V. Estrela, J. Hemanth, O. Saotome, G. Nikolakopoulos, R. Sabatini, vol. 2, 9, (IET, London, 2020), pp. 177–212
36. N. Razmjooy, V.V. Estrela, H.J. Loschi, A study on metaheuristic-based neural networks for image segmentation purposes, in *Memon QA*, ed. by S. A. Khoja, (Data Science – Theory, Analysis and Applications, 2019). https://doi.org/10.1201/9780429263798-2
37. R. Laptik, D. Navakauskas, Application of ant colony optimization for image segmentation. Elektronika Ir Elektrotechnika **80**, 13–18 (2015)
38. S. Sengupta, N. Mittal, M. Modi, Improved skin lesion edge detection method using ant colony optimization. Skin research and technology: Official journal of International Society for Bioengineering and the Skin (ISBS) [and] International Society for Digital Imaging of Skin (ISDIS) [and] International Society for Skin Imaging (2019)
39. N. Razmjooy, M. Ashourian, M. Karimifard, V.V. Estrela, H.J. Loschi, D. do Nascimento, R.P. França, M. Vishnevski, *Computer-aided diagnosis of skin cancer: A review* (Current Medical Imaging, Bentham Science Publishers, Sharjah, 2020). https://doi.org/10.2174/1573405616666200129095242
40. S. Bosse, D. Maniry, K. Müller, T. Wiegand, W. Samek, Deep Neural Networks for no-reference and full-reference image quality assessment. IEEE Trans. Image Process. **27**, 206–219 (2018)
41. S. Chakraborty, S. Chatterjee, A. Chatterjee, K. Mali, S. Goswami, S. Sen, Automated breast cancer identification by analyzing histology slides using metaheuristic supported supervised classification coupled with bag-of-features. 2018 Fourth International Conference on Research in Computational Intelligence and Communication Networks (ICRCICN), 81–86 (2018)
42. L. Duan, F. Xu, Y. Qiao, D. Zhao, T. Xu, C. Wu, An automated method with attention network for cervical cancer scanning. In: Proceedings of the Second Chinese Conference on Pattern Recognition and Computer Vision, Part II, PRCV 2019, Springer. (2019)